2015

Porous Layers Composed of Oxide Crystallites Formed by the Combination of Laser Ablation and Anodization of Metal

Abbie S. Ganas
West Chester University of Pennsylvania

Dmitry A. Znamensky
West Chester University of Pennsylvania

Nahúm Méndez Alba
Universidad Autónoma Metropoplitana-Iztapalapa

José Luis Hernández-Pozos
Universidad Autónoma Metropoplitana-Iztapalapa

Kurt W. Kolasinski
West Chester University of Pennsylvania, kkolasinski@wcupa.edu

Recommended Citation
Ganas, A. S., Znamensky, D. A., Alba, N. M., Hernández-Pozos, J. L., & Kolasinski, K. W. (2015). Porous Layers Composed of Oxide Crystallites Formed by the Combination of Laser Ablation and Anodization of Metal. *ECS Transactions, 69*(2), 155-160.
http://dx.doi.org/10.1149/06902.0155ecst

ECS Transactions 69(2): 155-160 (2015)

Porous Layers Composed of Oxide Crystallites Formed by the Combination of Laser Ablation and Anodization of Metal

Abbie S. Ganas[a], Dmitry A. Znamensky[a], Nahúm Méndez Alba[b], José Luis Hernández-Pozos[b], and Kurt W. Kolasinski[a]

[a] Department of Chemistry, West Chester University, West Chester, PA 19383-2, USA
[b] Departamento de Física, Universidad Autónoma Metropoplitana-Iztapalapa, Av. San Rafael Atlixco No 186, Col Vicentina, Del Iztapalapa, 09340, México D.F., México

High-voltage anodization is well known for producing nanostructures such as porous alumina and TiO_2 nanotubes. The formation mechanisms involve an intricate balance between oxide growth and dissolution in which pore initiation and propagation is convoluted with the need for strain relief. Laser ablation with a nanosecond pulsed Nd:YAG laser (532 nm) produces texture e.g. arrays of pillars, macropores and ripples. Nanoparticles produced in the ablation plume can also be deposited on the target or a remote substrate. These substrates are anodized in solutions typically used for porous film and nanotube production (including viscous fluoride-containing electrolytes). A number of metals have been investigated, with emphasis here on Al and Ti as well as Zn. Laser pre-texturing results in the formation of structures unattainable by anodization alone. Deposited nanoparticles of Al and Zn are found to act as seeds for the growth of oxide crystallites that fuse into porous crystallite films.

Introduction

In this paper, we report what we believe to be the first instance of room temperature formation of nanocrystalline alumina through a combination of nanoparticle deposition and electrochemical anodization of the substrate unto which the nanoparticles are deposited. Nanoparticles are generated in the plume created by laser ablation of a polycrystalline metal foil. Thin films of metal oxides such as porous Al_2O_3 and TiO_2 nanotubes are commonly formed by anodization in which the balance between etching and oxide growth is responsible for structure formation (1). Previous studies have shown the elegance and efficiency of either a one-step or two-step anodization (2-6). These films are amorphous as formed. The most common and general route to the formation of polycrystalline thin films of these oxides is to anneal the as-formed film. Here we report that anodization can lead to formation of crystalized oxidized aluminum at room temperature in the absence of annealing. The key to this process is the presence of Al nanocrystals, which act as seeds for the growth of the oxide crystallites. The Al nanocrystals are formed in a laser ablation plume. We demonstrate that crystalline oxide films can be grown from the nanoparticles when they are (i) deposited on the laser ablation target, (ii) deposited on an Al substrate remote from the laser ablation target, and (iii) deposited on a Ti substrate remote from the laser ablation target. We believe that large Al nanocrystals (>20 nm in diameter) act as seeds; whereas the majority of small Al nanocrystals (< 5 nm) act as feedstock for the initial growth stage of the oxide crystallites.

Laser irradiation close to the ablation threshold readily produces texture in the surface of the irradiated substrate (7-9). A variety of structures including ripples, pillars and pores can be formed depending on a number of parameters including laser power, number of shots, and gas pressure and composition above the sample (10). Structure formation on silicon (11-14), titanium (15), and germanium (12, 16) has been investigated in some detail in our lab with both nanosecond and femtosecond pulsed lasers.

Laser ablation is always accompanied by plume formation, which results from the ejection of atoms and clusters from the target. The extent of the plume and its collision dynamics depend on gas pressure and composition in the chamber above the target, the laser fluence, and the material being ablated (17-19). The temperature of the plume is initially several thousand kelvin; but as the particles relax radiatively and collisionally they condense and eventually solidify. Depending on the pressure in the chamber during the ablation process, these particles can either redeposit on the surface of the metal or precipitate within the chamber. Both processes occur at all pressures but the proportion of redeposition compared to remote deposition increases as the pressure increases.

Experimental

High purity 0.20 mm thick polished metal foils were obtained from Goodfellow (Al 99.0%, Ti 99.6%) or Baker (Zn ribbon "Baker analyzed"). These foils were cut into approximately 1 cm^2 pieces and cleaned through sonication with acetone and ethanol for five min in each solvent. All samples were irradiated with a Nd:YAG laser (SpectraPhysics Indi producing 160 mJ at 532 nm in 6–7 ns pulses and a 20 Hz repetition rate). The laser fluence onto the sample is adjusted to just above the ablation threshold by the positioning a 50 cm lens. The samples are held within a stainless steel vacuum chamber pumped by an alumina-trapped mechanical pump. During ablation, the vacuum chamber was purged with flowing argon gas. The target was translated linearly at a speed of 0.04 mm s^{-1} during laser irradiation to expose a stripe on the target to a sufficient number of laser shots. During laser ablation Ar is allowed to flow through the chamber to maintain a steady-state pressure of either 20 mbar (which we will call low pressure conditions) or 200 mbar (high pressure). During deposition onto a remote substrate, the chamber is pumped to approximately 1 mbar in the absence of Ar flow. After irradiation, samples were inspected with scanning electron microscopy (SEM) then anodized.

Anodization of Ti and Zn was performed in a well-stirred electrolyte of 0.3 wt% NH_4F/ ethylene glycol contained in a Teflon beaker held at 273 K by contact with an ice/water bath. Aluminum was anodized with this electrolyte or in 0.5 M H_2SO_4. A platinum foil is used as the cathode. An Agilent E3612A power supply was operated in a constant voltage mode during anodization. Ballast resistors added to the circuit were used to limit the maximum current. Anodization durations were between 2–27 hours for all samples. After anodization, all samples were rinsed first three times in ethanol and finally once in acetone. After rinsing, the samples were dried in a flow of He/N_2 or Ar.

After laser ablation and anodization, all samples were imaged with secondary electron scanning electron microscopy (SEM) images obtained in an FEI Quanta 400 Environmental SEM operating at 20 kV in high vacuum mode and using an Everhardt-Thornley detector. In order to determine the crystallinity of the aluminum particles,

imaging and selective area diffraction were performed with an FEI Tecnai T12T transmission electron microscope (TEM) operating at 120 kV.

Results and Discussion

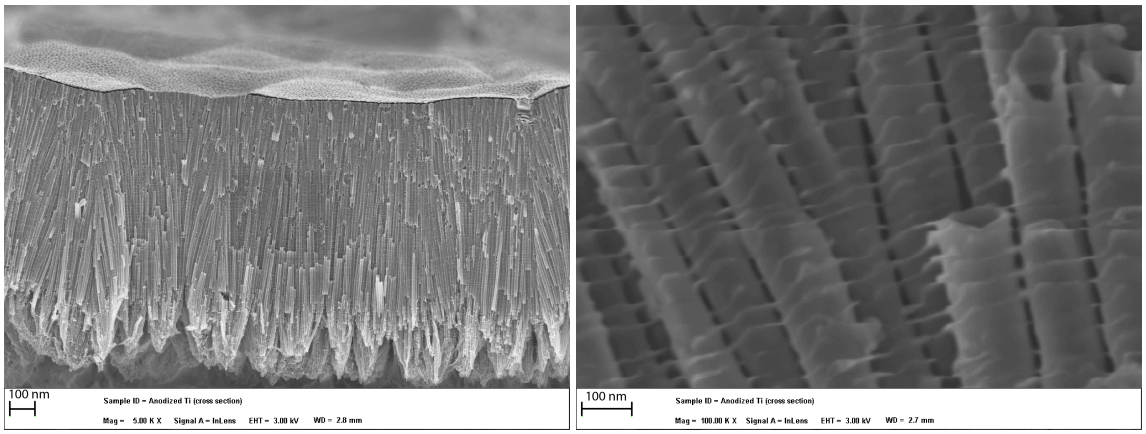

Figure 1 TiO_2 nanotubes shown in cross section at (a) low and (b) high magnification.

Anodization as described above was performed on three different types of metal substrates. When performed on unablated Al or Ti, anodization leads to the formation of porous alumina or TiO_2 nanotubes as reported in the literature (2-6). Figure 1 displays typical images of TiO_2 nanotubes consistent with those reported in the literature (2, 3). The new procedure reported here are that we have also anodized laser ablated substrates or substrates upon which nanoparticles have been deposited.

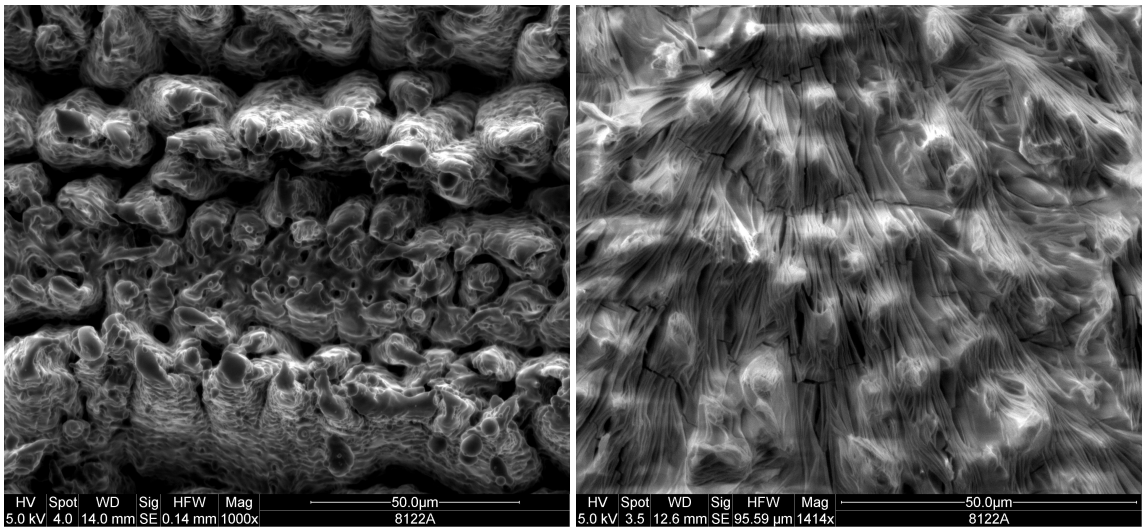

Figure 2(a) Plan view SEM micrograph of Al pillars produced by laser ablation in 200 mbar Ar background pressure. (b) Structure formed in the same sample after anodization in 0.5 M H_2SO_4 for 4 h.

Figure 2(a) exhibits the topology of an Al substrate that has been irradiated with the Nd:YAG laser. The region of the substrate irradiated with the high intensity portion of the laser beam profile exhibits an irregular array of more or less conical pillars. The sample appears black to the eye. When anodized at 20 V the topology is modified as shown in Fig. 2(b). Remnants of the pillars can be found. Surprisingly, oxidation has lead

to a tissue like appearance. Higher resolution images reveal that the aluminum oxide has cleaved into sheets as thin as 50 nm in width. No evidence of pore formation is found. Some combination of the damage introduced by laser ablation and the initial pillar morphology has completely changed the structure formation dynamics. The open structure shown in Fig. 2(a) certainly opens up new avenues for strain relief as the oxide grows. The imposition of pillars upon the natural length scale of growth instabilities normally associated with anodiziation under these conditions has changed the growth mode from a pore-formation regime to a cleaved-sheet regime.

Laser ablation produces nanoparticles within the ablation plume (17, 20). The structure of deposited nanoparticles depends sensitively on the deposition conditions. When Al was deposited at low density on a TEM grid, we found many nanoparticles with diameters of ≤ 5 nm. In addition, a few larger nanoparticles were found, most in the 20–100 nm range but some even larger. Observation of distinct diffraction spots from the 20 nm and larger nanoparticles indicates that Al nanoparticles are crystalline. However, Ti nanocrystals have not been found to exhibit sharp diffraction patterns. When deposited at higher density, the nanoparticles aggregate into structures such as those shown in the SEM image of Fig. 2(a). Most of the features shown in Fig. 2(a) are agglomerations of much smaller particles. At even higher loading, Fig. 2(b), the agglomerated features turn into cauliflower like structures. At even higher loading the cauliflower structures grow in height. Such features are found on both Al and Ti substrates.

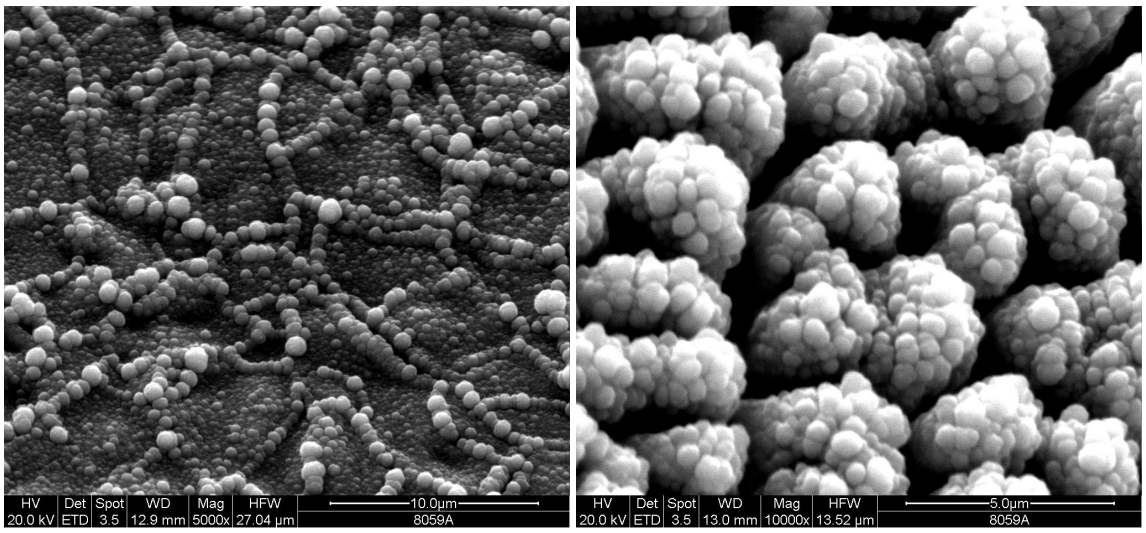

Figure 3 SEM micrographs of Ti nodules 50–750 nm in diameter at (a) lower and (b) higher packing density. The particles are redeposited on the ablation target. The density of redeposition decreases with distance away from the center of the stripe made by the incident laser.

When nanoparticle-decorated Al substrates were anodized, a completely different film structure is found compared to the pillar-covered region. Nanocrystallites of oxide are formed. As anodization continues, these nanocrystallites grow and eventually fuse. Figure 4 shows the regular shapes and flat angled faces that are clear indications of crystalline character. These aluminum oxide crystallites have only been observed in regions of the crystal that are initially covered with nanoparticles. They have been observed on ablated Al substrates in regions where the nanoparticles were redeposited

from the ablation plume. They have been observed on nonablated Al substrates upon which the nanoparticles precipitated after ablation of an Al target. They have also been observed on a Ti substrate upon which Al nanoparticles were deposited by laser ablation of an Al target. In the latter case, the aluminum oxide crystallites only grew until the deposited Al has all been oxidized. The crystalline Al nanoparticles were clearly acting as seeds that template for the formation of aluminum oxide crystallites. The low density of oxide crystallites formed most likely indicated that the larger (>20 nm) Al nanocrystals were acting as the seeds rather than the much more numerous ≤ 5 nm Al nanocrystals.

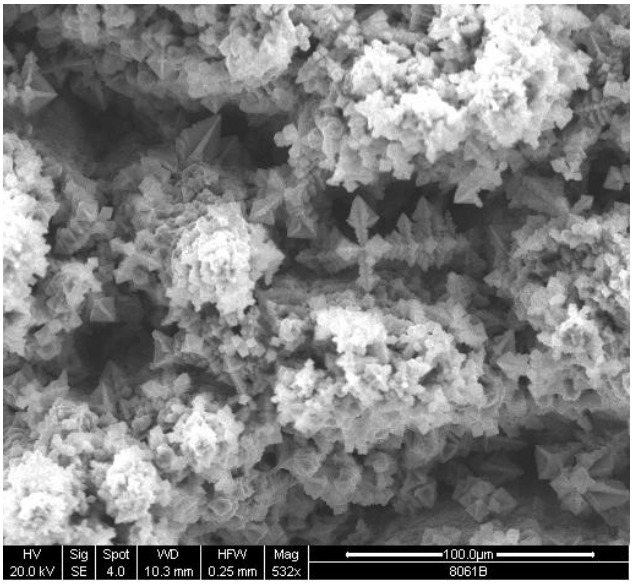

Figure 4 Aluminum oxide scepters formed by anodization of nanocrystal-decorated Al substrates for 2 h at 60 V in NH_3F/ethylene glycol.

When Ti was decorated with nanoparticles and then anodized in NH_3F/ethylene glycol, the surface was initially covered with fuzzy debris. However this soon cleared and nanotube formation occured just as it would on a non-decorated surface. The behavior of a Zn substrate decorated with Zn nanoparticles was much closer to that of aluminum. Preliminary results indicated the formation of oxide crystallites at low coverage. Furthermore, the regions in which these nanocrystals formed exhibited near-white-light photoluminescence when this region was illuminated with 254 nm light.

Conclusion

The combination of laser ablation with anodization or nanoparticle decoration prior to anodization allows us to access structure formation regimes that are unobtainable by anodization alone. It appears that nanocrystals of metal can act as templates that seed the formation of oxide nanocrystals that then grow into much larger structures. We highlight here our results with aluminum oxide structures formed by anodization of laser ablation pillars and Al-nanocrystal-decorated substrates. In the former case, a tissue-like structure of cleaved planes is formed. In the latter case, an intricate porous film of crystallites is formed. Nanocrystalline zinc oxide structures have also been formed which exhibit photoluminescence under UV irradiation.

Acknowledgement

We thank Mr P. Schaut, Dr. Fred Monson and the Center for Microanalysis and Imaging Research and Training (CMIRT) at WCU for their assistance. This article is dedicated to Yukio Ogata, who was a leader in porous silicon science, a gracious host and someone KWK is proud to have called a colleague.

References

1. K. R. Hebert, S. P. Albu, I. Paramasivam and P. Schmuki, *Nature Mater.*, **11** (2), 162 (2012).
2. A. Ghicov and P. Schmuki, *Chem. Commun.*, (20), 2791 (2009).
3. K. Lee, A. Mazare and P. Schmuki, *Chem. Rev.*, **114** (19), 9385 (2014).
4. W. Lee and S.-J. Park, *Chem. Rev.*, **114**, 7487−7556 (2014).
5. A. E. Mohamed and S. Rohani, *Energy & Environmental Science*, **4** (4), 1065 (2011).
6. H. Chik and J. M. Xu, *Mater. Sci. Eng., R*, **43** (4), 103 (2004).
7. B. K. Nayak and M. C. Gupta, *Optics and Lasers in Engineering*, **48** (10), 940 (2010).
8. E. Haro-Poniatowski, E. Fort, J. P. Lacharme and C. Ricolleau, *Appl. Phys. Lett.*, **87** (14), 143103 (2005).
9. T. Baldacchini, J. E. Carey, M. Zhou and E. Mazur, *Langmuir*, **22** (11), 4917 (2006).
10. K. W. Kolasinski, *Curr. Opin. Solid State Mater. Sci.*, **11** (5-6), 76 (2007).
11. D. Riedel, J. L. Hernández-Pozos, K. W. Kolasinski and R. E. Palmer, *Appl. Phys. A*, **78** (3), 381 (2004).
12. B. K. Nayak, M. C. Gupta and K. W. Kolasinski, *Appl. Surf. Sci.*, **253** (15), 6580 (2007).
13. D. Mills, T. Kreouzis, A. Sapelkin, B. Unal, N. Zyuzikov and K. W. Kolasinski, *Appl. Surf. Sci.*, **253** (15), 6575 (2007).
14. K. W. Kolasinski, M. E. Dudley, B. K. Nayak and M. C. Gupta, *Proc. SPIE-Int. Soc. Opt. Eng.*, **6586**, 65860H (2007).
15. B. K. Nayak, M. C. Gupta and K. W. Kolasinski, *Appl. Phys. A*, **90** (3), 399 (2008).
16. B. K. Nayak, M. C. Gupta and K. W. Kolasinski, *Nanotechnology*, **18** (19), 195302 (2007).
17. C. P. Wu and L. V. Zhigilei, *Appl. Phys. A*, **114** (1), 11 (2014).
18. E. Leveugle, D. S. Ivanov and L. V. Zhigilei, *Appl. Phys. A*, **79** (7), 1643 (2004).
19. L. V. Zhigilei, *Appl. Phys. A*, **76** (3), 339 (2003).
20. R. Q. Guo, J. Nishimura, M. Ueda, M. Higashihata, D. Nakamura and T. Okada, *Appl. Phys. A*, **89** (1), 141 (2007).